Applied Physics Letters

Limitations of In_2O_3 as a transparent conducting oxide

Cite as: Appl. Phys. Lett. **115**, 082105 (2019); https://doi.org/10.1063/1.5109569
Submitted: 09 May 2019 . Accepted: 04 August 2019 . Published Online: 23 August 2019

H. Peelaers, E. Kioupakis, and C. G. Van de Walle

Applied Physics Letters ARTICLE scitation.org/journal/apl

Limitations of In_2O_3 as a transparent conducting oxide

Cite as: Appl. Phys. Lett. **115**, 082105 (2019); doi: 10.1063/1.5109569
Submitted: 9 May 2019 · Accepted: 4 August 2019 ·
Published Online: 23 August 2019

H. Peelaers,[1,2,a)] E. Kioupakis,[3] and C. G. Van de Walle[1]

AFFILIATIONS

[1]Materials Department, University of California, Santa Barbara, California 93106-5050, USA
[2]Department of Physics and Astronomy, University of Kansas, Lawrence, Kansas 66045, USA
[3]Department of Materials Science and Engineering, University of Michigan, Ann Arbor, Michigan 48109, USA

[a)]Electronic mail: peelaers@ku.edu

ABSTRACT

Sn-doped In_2O_3 or ITO is the most widely used transparent conducting oxide. We use first-principles calculations to investigate the limitations to its transparency due to free-carrier absorption mediated by phonons or charged defects. We find that the main contribution to the phonon-assisted indirect absorption is due to emission (as opposed to absorption) of phonons, which explains why the process is relatively insensitive to temperature. The wavelength dependence of this indirect absorption process can be described by a power law. Indirect absorption mediated by charged defects or impurities is also unavoidable since doping is required to obtain conductivity. At high carrier concentrations, screening by the free carriers becomes important. We find that charged-impurity-assisted absorption becomes larger than phonon-assisted absorption for impurity concentrations above 10^{20} cm^{-3}. The differences in the photon-energy dependence of the two processes can be explained by band structure effects.

In_2O_3 and, in particular, Sn-doped In_2O_3 (usually referred to as ITO), is the most widely used transparent conducting oxide (TCO).[1] The material combines transparency to visible light with high conductivity, allowing for a wide range of applications, such as transparent electrodes in flat-panel displays[2] or solar cells,[3] (opto)electronic devices,[4] IR-reflective window coatings,[5] plasmonics,[6] and integration with Ga_2O_3 electronics.[7]

The fundamental bandgap of In_2O_3 is around 2.6–2.9 eV;[8–13] however, strong optical absorption starts only around 3.5–3.7 eV.[8–13] The absence of absorption from the valence to conduction band is a necessary but not sufficient condition for transparency to visible light. Achieving high conductivity requires introducing a high concentration of electrons in the conduction band; carrier concentrations as high as 2×10^{21} cm^{-3} have been reported.[14] Excitation of these free carriers to higher-energy states can also lead to optical absorption; a fundamental study of this process is the subject of this letter.

Direct transitions of free carriers in the conduction band to higher-lying conduction bands (see Fig. 1) are not possible with visible-light photons; only indirect transitions can lead to absorption within the visible range. Such processes are usually described by a Drude model; here, we will use first-principles calculations, i.e., without any fitting parameters, to go beyond such a phenomenological approach. This allows us to describe the fundamental limitations to the transparency of In_2O_3 caused by the interactions of phonons and charged impurities (or defects) with the free carriers. We will first discuss the phonon-assisted process, followed by a discussion of the effect of charged impurities, which are unavoidably present due to the need for large concentrations of free carriers to obtain good conductivity. For the phonon-assisted process, we compare our results, based on first-principles calculations of matrix elements, with the commonly used Fröhlich approximation, and we discuss why absorption in In_2O_3 is much weaker than in SnO_2. We explicitly include screening, for both the phonon-assisted and charged-impurity processes.

Our calculations are performed using density functional theory within the local-density approximation (LDA).[15] We used norm-conserving Troullier-Martins pseudopotentials[16] in the QUANTUM-ESPRESSO[17] package, with a cutoff energy of 90 Ry for the plane wave basis. The Brillouin zone is sampled with a $4 \times 4 \times 4$ Monkhorst-Pack[18] **k**-point mesh. Phonons and electron-phonon coupling matrix elements are calculated within density functional perturbation theory[19] on a $24 \times 24 \times 24$ **q**-grid.

In_2O_3 can occur in several polymorphs;[20] here, we focus on the most stable structure, which is cubic bixbyite, with space group #206 or $Ia\bar{3}$. Its unit cell, shown in Fig. 2,[30] consists of 40 atoms. We obtain

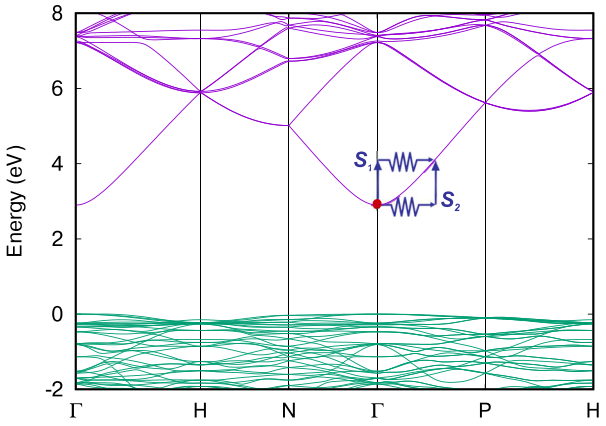

FIG. 1. The electronic band structure of In_2O_3 along high-symmetry **k**-point paths. The zero energy is set at the valence-band maximum. The transitions corresponding to the $\boldsymbol{S}_1$ and $\boldsymbol{S}_2$ matrix elements [Eq. (2)] are illustrated.

a lattice parameter of 10.15 Å, in good agreement with the experimental value of 10.12 Å.[21] Since there are 40 atoms in the unit cell, 120 phonon modes are present, which significantly increases the computational burden of calculating the electron-phonon interactions on a fine **q**-point mesh. Our calculated frequencies at the Γ point agree well with previous calculations[22] and with experiment.[22–29] A comparison of the Raman-active phonon frequencies is shown in the supplementary material in Table S1.

The electronic band structure is shown in Fig. 1. Since LDA underestimates the bandgap, a scissor shift is applied to the conduction bands to reproduce the experimental bandgap. However, since we are only considering free-carrier absorption here, the exact value of the bandgap is not important; what matters is the conduction-band structure. To ascertain the validity of the LDA conduction-band structure, we compared it with a calculation performed with a hybrid functional.[31] The energy and dispersion of conduction bands were very similar in the two calculations, with differences that would have negligible effects on the calculated free-carrier absorption (see Fig. S1 of the supplementary material). Figure 1 shows that the conduction-band minimum is located at the Γ point. The valence bands have low dispersion and mainly O *p* character, while the lowest conduction band is composed of *s* orbitals and has a large dispersion. The electron effective mass calculated from LDA, $0.16\,m_e$, is close to the experimental value of $0.18\,m_e$.[32]

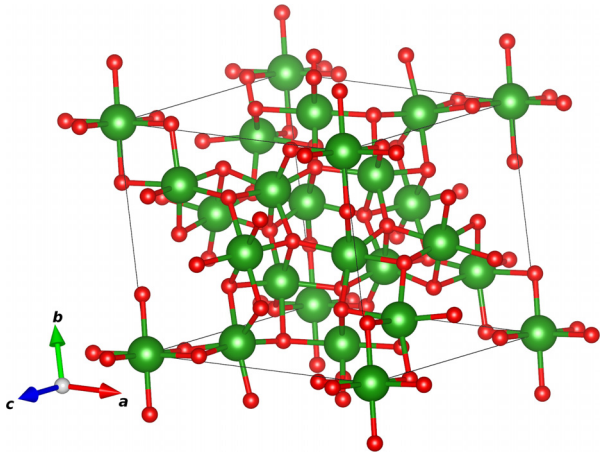

FIG. 2. The 40-atom unit cell of bixbyite In_2O_3. The large spheres are In atoms and the smaller spheres are O atoms. Indium atoms occupy distorted octahedral positions on either the Wyckoff 24*d* or 8*d* sites and oxygen atoms occupy the 48*e* positions.

Phonons mediate absorption by providing the momentum necessary to reach unoccupied conduction-band states away from the zone center. We describe this indirect absorption process using Fermi's golden rule[33]

$$\alpha(\omega) = 2\frac{4\pi^2 e^2}{\omega c n_r(\omega)}\frac{1}{V_{\text{cell}}}\frac{1}{N_{\boldsymbol{k}}N_{\boldsymbol{q}}}\sum_{\nu ij\boldsymbol{kq}}|\hat{\boldsymbol{e}}\cdot(\boldsymbol{S}_1+\boldsymbol{S}_2)|^2 \times P\delta(\epsilon_{j,\boldsymbol{k}+\boldsymbol{q}}-\epsilon_{i\boldsymbol{k}}-\hbar\omega\pm\hbar\omega_{\nu\boldsymbol{q}}). \quad (1)$$

Here, V_{cell} is the unit-cell volume, $\hbar\omega$ and $\hat{\boldsymbol{e}}$ the energy and polarization of the absorbed photon, $n_r(\omega)$ the refractive index of In_2O_3 at frequency ω, $\hbar\omega_{\nu\boldsymbol{q}}$ the phonon energy, and $\epsilon_{i\boldsymbol{k}}$ the electron energy. *i* and *j* indicate the band number, ν the phonon mode, $\boldsymbol{k}$ and $\boldsymbol{q}$ the wave vectors, and $N_{\boldsymbol{k}}$ and $N_{\boldsymbol{q}}$ the number of $\boldsymbol{k}$ and $\boldsymbol{q}$ wave vectors in the grid. The generalized optical matrix elements $\boldsymbol{S}_1$ and $\boldsymbol{S}_2$ are given by

$$\boldsymbol{S}_1(\boldsymbol{k},\boldsymbol{q}) = \sum_m \frac{\boldsymbol{v}_{im}(\boldsymbol{k})g^{\text{el-ph}}_{mj,\nu}(\boldsymbol{k},\boldsymbol{q})}{\epsilon_{m\boldsymbol{k}}-\epsilon_{i\boldsymbol{k}}-\hbar\omega},$$
$$\boldsymbol{S}_2(\boldsymbol{k},\boldsymbol{q}) = \sum_m \frac{g^{\text{el-ph}}_{im,\nu}(\boldsymbol{k},\boldsymbol{q})\boldsymbol{v}_{mj}(\boldsymbol{k}+\boldsymbol{q})}{\epsilon_{m,\boldsymbol{k}+\boldsymbol{q}}-\epsilon_{i\boldsymbol{k}}\pm\hbar\omega_{\nu\boldsymbol{q}}}, \quad (2)$$

and correspond to the two possible paths of the indirect absorption process (see Fig. 1). $\boldsymbol{v}_{im}(\boldsymbol{k})$ are the optical matrix elements and $g^{\text{el-ph}}_{mj,\nu}(\boldsymbol{k},\boldsymbol{q})$ the electron-phonon coupling matrix elements. The factor *P* accounts for the carrier and phonon statistics and contains the temperature dependence,

$$P = \left(n_{\nu\boldsymbol{q}}+\frac{1}{2}\pm\frac{1}{2}\right)(f_{i\boldsymbol{k}}-f_{j,\boldsymbol{k}+\boldsymbol{q}}). \quad (3)$$

Here, $n_{\nu\boldsymbol{q}}$ and $f_{i\boldsymbol{k}}$ are the phonon and electron occupation numbers. The upper (lower) sign corresponds to phonon emission (absorption). Note that all quantities entering here are calculated from first principles, without any fitting parameters. Equation (1) contains a sum over both **k**- and **q**-points. By making the assumption that all free carriers are located near the Γ point and that these have similar electron-phonon matrix elements, we can replace the double sum by a single sum over **q**-points, which is essential for rendering the computations tractable. The assumption that the carriers are located near the Γ point is fully justified for electron concentrations up to $3\times10^{18}\,\text{cm}^{-3}$, while the assumption for the matrix elements is valid for Fermi levels up to at least 0.5 eV above the conduction-band minimum (corresponding to carrier concentrations up to $2\times10^{20}\,\text{cm}^{-3}$). To obtain results that are independent of the free-carrier concentration, we will report the absorption cross section, which is the absorption coefficient α divided by the free-carrier concentration.

There are two possible processes: either an existing phonon can be absorbed or a new phonon can be emitted. Our results (at 300 K) are shown in Fig. 3 for photon energies up to 3.7 eV, the energy at

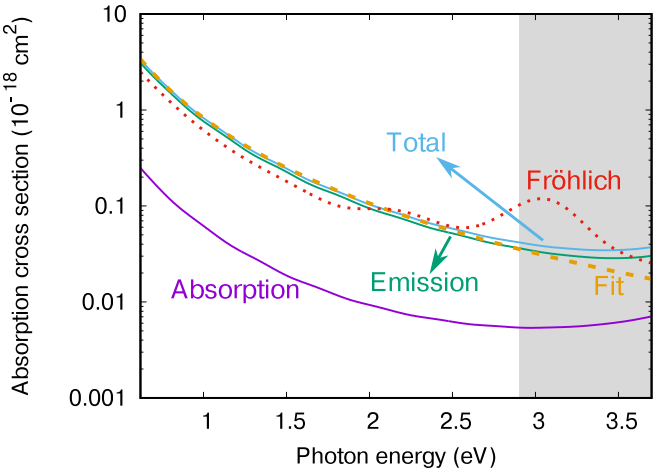

FIG. 3. Calculated phonon-assisted absorption cross section for In_2O_3 (at 300 K) as a function of photon energy. The gray area indicates energies for which weak across-the-gap transitions can take place. Contributions from phonon absorption vs phonon emission are identified. The dashed line indicates a fit to a power law, as described in the text. The dotted line indicates the result obtained by the Fröhlich model.

which strong absorption from the valence to conduction bands sets in. However, weak across-the-gap absorption has been observed with an onset at the fundamental gap;[8,34] therefore, we shade the energy range between 2.9 and 3.7 eV in gray. The phonon emission process is clearly the dominant absorption process at 300 K. This also implies that lowering the temperature would not significantly affect phonon-assisted absorption, since phonons can be emitted even at 0 K. Figure S2 shows a comparison between 0 K and 300 K.

The indirect absorption increases with decreasing photon energy (or longer photon wavelength). We find that the relation between phonon-assisted indirect absorption and photon energy can be expressed by a power law. In Fig. 3, we show a fit to $\sigma/(10^{-18}\text{cm}^2) = a \times (\hbar\omega/\text{eV})^{-3}$, where we fitted in the region of photon energies from 0.62 eV to 2.7 eV. The fit yields a coefficient $a = 0.83$. The agreement between the first-principles results and the fit is very good at low photon energies; deviations are observed only for photon energies larger than 2.5 eV. This fit implies that the absorption is inversely proportional to the cube power of the photon energy or equivalently proportional to the cube of the photon wavelength. Such a relationship is expected in the case of linear dispersion (a good approximation for conduction bands that show strong nonparabolicity) and absorption dominated by longitudinal-optical (LO) phonons.[35]

Our first-principles results in Fig. 3 take all phonon modes and all possible transitions between electronic bands into account. It is informative to compare these results with a simplified model, in which we assume that the main contribution to phonon-assisted absorption is due to LO phonon modes and that only the highest phonon mode contributes. The electron-phonon coupling matrix elements are then given by the Fröhlich model

$$g_F(\boldsymbol{q}) = \frac{1}{q}\sqrt{\frac{2\pi\hbar\omega_{\text{LO}}e^2}{V_{\text{cell}}}\left(\frac{1}{\epsilon_\infty}-\frac{1}{\epsilon_0}\right)}, \tag{4}$$

where ω_{LO} is the frequency of the LO mode at the Γ point and ϵ_∞ and ϵ_0 are the high-frequency and static dielectric constants. For photon energies up to about 2 eV, where intraband transitions dominate, the single-LO phonon mode Fröhlich model closely approximates the full first-principles results. The slight underestimation is related to the fact that not all modes are taken into account. Nevertheless, the good agreement indicates that LO phonon modes, with a $1/q$ dependence of the electron-phonon matrix elements, are dominant.

The absorption cross section calculated by the Fröhlich model shows a slight upturn at energies just below 2 eV, which is caused by interband processes: an inspection of the band structure (Fig. 1) shows that at energies of about 2 eV above the conduction-band minimum, the first conduction band becomes degenerate with the second conduction band, for example, along the segment H-N. However, the Fröhlich model overestimates the magnitude of these interband electron-phonon matrix elements, which is even more evident for interband transitions around 3 eV.

The Fröhlich model also provides insight into why phonon-assisted indirect absorption in In_2O_3 is about 50% smaller compared to SnO_2,[33,35] another TCO material. Based on Eq. (4), we see that electron-phonon coupling is stronger in SnO_2. SnO_2 is more ionic than In_2O_3, i.e., there is a larger difference between the static and high-frequency dielectric constants, and hence, the factor $\left(\frac{1}{\epsilon_\infty}-\frac{1}{\epsilon_0}\right)$ in the Fröhlich model [Eq. (4)] is larger in SnO_2. In addition, the highest LO phonon frequency in SnO_2 is larger than the highest LO frequency in In_2O_3. Both effects contribute to SnO_2 having stronger absorption than In_2O_3. However, an even larger role is played by the density of states [which enters Eq. (1) through the energy-conserving delta function] being larger in SnO_2 than in In_2O_3, due to the smaller effective mass for electrons of In_2O_3.

At high carrier concentrations, screening of the electron-phonon interaction can be significant. This effect is included by multiplying the electron-phonon matrix elements by $\frac{q^2}{q^2+q_{\text{scr}}^2}$. q_{scr} is a screening length, which is obtained from either the Debye model (nondegenerate case) or the Thomas-Fermi model (degenerate case). The results are shown in Fig. 4 for two values of the electron concentration. The curve

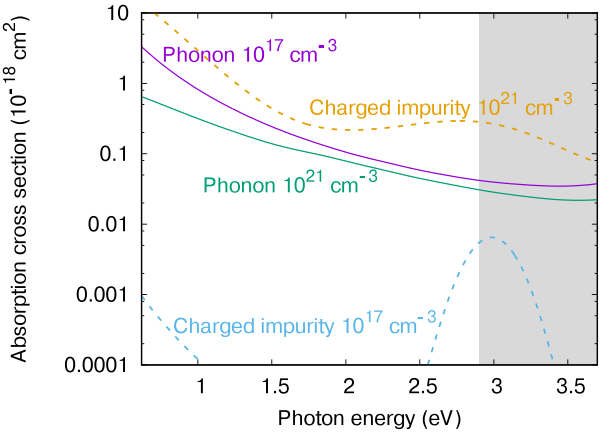

FIG. 4. Phonon- (solid lines) and charged-impurity-assisted (dashed lines) absorption cross section for In_2O_3 as a function of photon energy, for two representative concentrations of free carriers. Screening is included as described in the text.

labeled "Phonon 10^{17} cm^{-3}" in Fig. 4 is practically equivalent to the unscreened result (shown previously in Fig. 3), since for these low carrier concentrations, the effect of screening is negligible. At higher free-carrier concentrations, screening becomes important, reducing the phonon-assisted absorption cross section. The screening effect is larger for smaller photon energies.

We now turn to a discussion of free-carrier absorption assisted by a different mechanism, namely, charged-impurity scattering. This process is unavoidable, because the high conductivity of a TCO requires doping, which leads to the presence of ionized defects or impurities. In In_2O_3, the free carriers are typically provided by Sn doping, leading to the presence of charged Sn^+ centers. We describe the resulting indirect absorption process by scattering off a screened Coulomb potential, where the matrix elements are given by

$$g_{i,j}^{\text{impurity}} = \left\langle i, \boldsymbol{k} \left| \frac{4\pi e^2 Z}{\epsilon_0 (q^2 + q_{\text{scr}}^2)} \right| j, \boldsymbol{k} + \boldsymbol{q} \right\rangle. \quad (5)$$

We assume here that all Sn dopants are ionized and that these are the only charged impurities present; the concentration of ions is then equal to the concentration of free carriers. This assumption neglects compensation and thus provides a lower limit for the total concentration of charged centers.

As seen in Fig. 4, at 10^{17} cm^{-3}, charged-impurity-assisted absorption is negligible compared to the phonon-assisted process, but at 10^{21} cm^{-3}, charged-impurity scattering dominates. For photon energies up to 2 eV, the absorption decreases with increasing photon energies, similar to the phonon-assisted process. Above 2 eV, the impurity-assisted absorption increases, with a peak around 3 eV. As mentioned before, for energies around 2 eV above the conduction-band minimum, the first conduction band becomes degenerate with the second conduction band (Fig. 1). The corresponding matrix elements are larger for the charged-impurity process compared to the phonon process, leading to an increase in absorption. In addition, around 3 eV, many more final states become available (see, e.g., the band crossings at the H point in Fig. 1). Note that in the band structure obtained using hybrid functionals (see Fig. S1), the higher conduction bands are located at slightly higher energies compared to our LDA calculations; this will move the aforementioned peaks to higher energies. The crossover point, where the impurity-assisted process is similar in magnitude to the phonon-assisted process, occurs at an impurity concentration around 3×10^{20} cm^{-3}; at higher doping concentrations, the impurity-assisted process becomes the dominant absorption process.

In conclusion, we have reported a detailed analysis of the limitations on transparency due to indirect free-carrier absorption in In_2O_3. Using first-principles techniques, we find that the phonon-assisted process is dominated by the emission of phonons and increases with decreasing photon energies. This increase can be described by a third power dependence on the wavelength. For long-wavelength photons, a Fröhlich model, only taking the highest LO phonon mode into account, provides a reasonable description of the indirect absorption up to about 2.5 eV. This model can also explain why phonon-assisted indirect absorption in In_2O_3 is about 50% smaller than that in SnO_2. Charged-impurity-assisted absorption becomes the dominant process for concentrations above 3×10^{20} cm^{-3}.

See the supplementary material for a comparison of the band structure calculated with LDA and with a hybrid functional, a comparison of the calculated Raman-active phonon frequencies with previous calculations and experiments, and a comparison of the phonon-assisted indirect absorption at 0 K and 300 K.

This work was supported by the GAME MURI of the Air Force Office of Scientific Research (No. FA9550-18-1-0479). Computational resources were provided by the Extreme Science and Engineering Discovery Environment (XSEDE), which is supported by the National Science Foundation under Grant No. ACI-1548562.

REFERENCES

[1]K. Ellmer, Nat. Photonics **6**, 809 (2012).
[2]M. Katayama, Thin Solid Films **341**, 140 (1999).
[3]E. Fortunato, D. Ginley, H. Hosono, and D. C. Paine, MRS Bull **32**, 242 (2007).
[4]O. Bierwagen, Semicond. Sci. Technol. **30**, 024001 (2015).
[5]I. Hamberg and C. G. Granqvist, J. Appl. Phys. **60**, R123 (1986).
[6]X. Liu, J. Park, J. H. Kang, H. Yuan, Y. Cui, H. Y. Hwang, and M. L. Brongersma, Appl. Phys. Lett. **105**, 181117 (2014).
[7]H. Peelaers, D. Steiauf, J. B. Varley, A. Janotti, and C. G. Van de Walle, Phys. Rev. B **92**, 085206 (2015).
[8]R. L. Weiher and R. P. Ley, J. Appl. Phys. **37**, 299 (1966).
[9]C. Janowitz, V. Scherer, M. Mohamed, A. Krapf, H. Dwelk, R. Manzke, Z. Galazka, R. Uecker, K. Irmscher, R. Fornari, M. Michling, D. Schmeißer, J. R. Weber, J. B. Varley, and C. G. Van de Walle, New J. Phys. **13**, 085014 (2011).
[10]V. Scherer, C. Janowitz, A. Krapf, H. Dwelk, D. Braun, and R. Manzke, Appl. Phys. Lett. **100**, 212108 (2012).
[11]P. D. C. King, T. D. Veal, F. Fuchs, C. Y. Wang, D. J. Payne, A. Bourlange, H. Zhang, G. R. Bell, V. Cimalla, O. Ambacher, R. G. Egdell, F. Bechstedt, and C. F. McConville, Phys. Rev. B **79**, 205211 (2009).
[12]A. Walsh, J. Da Silva, S.-H. Wei, C. Körber, A. Klein, L. Piper, A. DeMasi, K. Smith, G. Panaccione, P. Torelli, D. Payne, A. Bourlange, and R. Egdell, Phys. Rev. Lett. **100**, 167402 (2008).
[13]A. J. Morris and B. Monserrat, Phys. Rev. B **98**, 161203 (2018).
[14]O. Bierwagen and J. S. Speck, Phys. Status Solidi A **211**, 48 (2014).
[15]D. Ceperley and B. Alder, Phys. Rev. Lett. **45**, 566 (1980); J. P. Perdew and A. Zunger, Phys. Rev. B **23**, 5048 (1981).
[16]N. Troullier and J. L. Martins, Phys. Rev. B **43**, 1993 (1991).
[17]P. Giannozzi, S. Baroni, N. Bonini, M. Calandra, R. Car, C. Cavazzoni, D. Ceresoli, G. L. Chiarotti, M. Cococcioni, I. Dabo, A. Dal Corso, S. de Gironcoli, S. Fabris, G. Fratesi, R. Gebauer, U. Gerstmann, C. Gougoussis, A. Kokalj, M. Lazzeri, L. Martin-Samos, N. Marzari, F. Mauri, R. Mazzarello, S. Paolini, A. Pasquarello, L. Paulatto, C. Sbraccia, S. Scandolo, G. Sclauzero, A. P. Seitsonen, A. Smogunov, P. Umari, and R. M. Wentzcovitch, J. Phys.: Condens. Matter **21**, 395502 (2009).
[18]H. Monkhorst and J. Pack, Phys. Rev. B **13**, 5188 (1976).
[19]S. Baroni, S. de Gironcoli, A. Dal Corso, and P. Giannozzi, Rev. Mod. Phys. **73**, 515 (2001).
[20]F. Fuchs and F. Bechstedt, Phys. Rev. B **77**, 155107 (2008).
[21]M. Marezio, Acta Crystallogr. **20**, 723 (1966).
[22]B. Garcia-Domene, H. M. Ortiz, O. Gomis, J. A. Sans, F. J. Manjón, A. Muñoz, P. Rodríguez-Hernández, S. N. Achary, D. Errandonea, D. Martínez-García, A. H. Romero, A. Singhal, and A. K. Tyagi, J. Appl. Phys. **112**, 123511 (2012).
[23]C. Kranert, R. Schmidt-Grund, and M. Grundmann, Phys. Status Solidi RRL **8**, 554 (2014).
[24]W. B. White and V. G. Keramidas, Spectrochim. Acta A **28**, 501 (1972).
[25]G. Korotcenkov, V. Brinzari, M. Ivanov, A. Cerneavschi, J. Rodriguez, A. Cirera, A. Cornet, and J. Morante, Thin Solid Films **479**, 38 (2005).
[26]C. Matei Ghimbeu, J. Schoonman, and M. Lumbreras, Ceram. Int. **34**, 95 (2008).
[27]Y. Zhang, J. Li, Q. Li, L. Zhu, X. Liu, X. Zhong, J. Meng, and X. Cao, Scr. Mater. **56**, 409 (2007).
[28]O. M. Berengue, A. D. Rodrigues, C. J. Dalmaschio, A. J. C. Lanfredi, E. R. Leite, and A. J. Chiquito, J. Phys. D: Appl. Phys. **43**, 045401 (2010).

[29]M. Rojas-López, J. Nieto-Navarro, E. Rosendo, H. Navarro-Contreras, and M. A. Vidal, Thin Solid Films **379**, 1 (2000).
[30]K. Momma and F. Izumi, J. Appl. Crystallogr. **44**, 1272 (2011).
[31]J. Heyd, G. E. Scuseria, and M. Ernzerhof, J. Chem. Phys. **124**, 219906 (2006).
[32]M. Feneberg, J. Nixdorf, C. Lidig, R. Goldhahn, Z. Galazka, O. Bierwagen, and J. S. Speck, Phys. Rev. B **93**, 045203 (2016).
[33]H. Peelaers, E. Kioupakis, and C. G. Van de Walle, Phys. Rev. B **92**, 235201 (2015).
[34]K. Irmscher, M. Naumann, M. Pietsch, Z. Galazka, R. Uecker, T. Schulz, R. Schewski, M. Albrecht, and R. Fornari, Phys. Status Solidi A **211**, 54 (2014).
[35]H. Peelaers, E. Kioupakis, and C. G. Van de Walle, Appl. Phys. Lett. **100**, 011914 (2012).